Available online at www.sciencedirect.com
ScienceDirect
International Journal of Thermal Sciences 48 (2009) 871–880
International Journal of Thermal Sciences
www.elsevier.com/locate/ijts

Heat transfer by natural convection, conduction and radiation in an inclined square enclosure bounded with a solid wall

H.F. Nouanegue, A. Muftuoglu, E. Bilgen *

École Polytechnique, Box 6079, centre ville, Montreal, QC, H3C 3A7, Canada

Received 3 October 2007; received in revised form 17 June 2008; accepted 18 June 2008

Available online 10 July 2008

Abstract

We study in this paper conjugate heat transfer by natural convection, conduction and radiation in an inclined square enclosure bounded by a solid wall with its outer boundary at constant temperature while the opposing active wall is with a constant heat flux. We solved two-dimensional coupled equations of conservation of mass, momentum and energy, with the Boussinesq approximation using finite difference method and the SIMPLER algorithm. Various parameters were: Rayleigh number from 10^8 to 3×10^{10}, dimensionless conductivity of bounding wall from 10 to 40 and dimensionless wall width from 0 to 0.15, aspect ratio equal to 1, the inclination angle 60 to 150° and the surface emissivity from 0 to 1. We presented the results in terms of heat flux and Nusselt number as a function of the Rayleigh number and other dimensionless parameters, as well as in terms of flow and temperature fields. We found that the interaction among the three modes of heat transfer was significant, the influence of the surface radiation on the natural convection was non-negligible and the flow and temperature fields as well as the heat transfer across the enclosure were modified.

Keywords: Conjugate heat transfer; Natural convection; Conduction; Radiation; Enclosure with massive wall

1. Introduction

Enclosures with bounding walls are encountered when simulating building components, in particular passive heating and cooling systems. In other applications, such as cooling of electronic components, various types of boards are used. In direct gain passive solar systems, the dwelling is simulated as a two dimensional enclosure having two vertical walls, one transparent and the other massive, which are bounded by two horizontal insulated boundaries. Heat transfer by a constant heat flux through the transparent vertical wall simulates solar radiation reception while a massive wall with an isothermal condition at the outer boundary simulates the adjacent building component at constant temperature at its outer boundary (e.g., [1]). In other applications like cooling of electronic components, we encounter similar systems, which consist always of a board with finite thickness and conductivity and heater with constant heat flux (e.g., [2]). Heat transfer in these systems is usually by combination of natural convection, conduction and radiation.

During the last two decades, various studies dealing with natural convection as well as natural convection—conduction in enclosures have been published (e.g., [3–6]). These studies have focused on the effect of geometrical parameters, the Rayleigh number, inclination angle on the heat transfer and flow field. In case of natural convection—conduction heat transfer, the conjugate transfer has been solved to study the influence of conduction on natural convection. In most of the cases, boundary conditions have been isothermal vertical walls and adiabatic horizontal walls. Few have also considered constant heat flux on one of the vertical walls simulating solar radiation.

There are several studies on conjugate heat transfer by natural convection and surface radiation (e.g., [7–12] and the references therein). Indirectly related to the problem encountered in passive systems, Akiyama and Chong [7] studied heat transfer by natural convection and radiation in a differentially heated square cavity in which two vertical walls were isothermal and the two horizontal walls adiabatic. They showed that the influence of radiation on natural convection was non-negligible.

* Corresponding author. Tel.: +1 514 340 4711, ext. 4579; fax: +1 514 340 5917.
E-mail address: bilgen@polymtl.ca (E. Bilgen).

1290-0729/$ – see front matter
doi:10.1016/j.ijthermalsci.2008.06.008

Nomenclature

A	enclosure aspect ratio, $= L/H$
A_j	surface area of element j ..... m^2
c_p	heat capacity ..... J/kg K
F_{ij}	configuration factor
g	acceleration due to gravity ..... m/s^2
H	cavity height ..... m
k	thermal conductivity ..... W/m K
k_r	conductivity ratio
L	cavity width ..... m
l	wall thickness ..... m
N_r	radiation number, $= \sigma T_\infty^4/q''$
Nu	Nusselt number
Nu_r	radiation Nusselt number, $= h_r H/k_f$
p	pressure ..... Pa
P	dimensionless pressure, $= (p - p_\infty)H^2/\rho\alpha_f^2$
Pr	Prandtl number, $= \upsilon/\alpha_f$
Q_j	power at element j ..... W
q''	heat flux ..... W/m^2
q	dimensionless heat flux, $= -\frac{\partial\theta}{\partial X} + N_r\zeta$
q_c	convective heat flux ..... W/m^2
q_r	radiative heat flux ..... W/m^2
q_t	combined heat flux ..... W/m^2
Ra	Rayleigh number, $= g\beta q'' H^4/(\upsilon\alpha_f k)$
t	time ..... s
U, V	dimensionless fluid velocities, $= uH/\alpha_f,\ vH/\alpha_f$
$\dot{V}$	volume flow rate through the vents in [11]
w	dimensionless wall thickness, $= \ell/H$
X, Y	dimensionless Cartesian coordinates, $= x/H,\ y/H$
x, y	Cartesian coordinates

Greek symbols

α	thermal diffusivity ..... m^2/s
α_r	thermal diffusivity ratio, $= \alpha_s/\alpha_f$
β	volumetric coefficient of thermal expansion 1/K
Γ	general diffusion coefficient
δ_{ij}	Kronecker delta
ε	surface emissivity
ζ	dimensionless radiative heat flux, $= q_r/\sigma T_\infty^4$
Θ	temperature ratio, $= T/T_\infty$
θ	dimensionless temperature, $= (T - T_\infty)/(Hq''/k)$
υ	kinematic viscosity ..... m^2/s
ρ	fluid density ..... kg/m^3
σ	Stefan–Boltzmann constant
τ	dimensionless time, $= \alpha t/H^2$
ψ	stream function
φ	inclination angle

Superscripts

–	average

Subscripts

c	convection
ext	extremum
f	fluid
i	c, r, t
r	radiation, ratio
s	solid
t	total or combined
∞	ambient value
1	at the left vertical boundary, $X = 0$
2	at the right vertical boundary, $X = A$

Ramesh and Venkateshan [8] studied experimentally the effect of surface radiation on heat transfer by natural convection in a differentially heated and horizontal walls insulated square cavity. They demonstrated that the surface radiation suppressed natural convection. Balaji and Venkateshan [9] studied numerically the interaction between surface radiation and natural convection in a square cavity and presented a parametric study on the effect of surface radiation. Mezrhab and Bchir [10,11] and Mezrhab et al. [12] studied numerically the conjugate heat transfer by three modes in a differentially heated square cavity containing a solid object and with its horizontal walls adiabatic. They reported that the solid object did not alter significantly the heat transfer rate through the cavity and they presented flow and temperature fields and overall heat transfer as a function of conductivity ratio, Rayleigh number and a geometric parameter.

The studies in [7–12] have been on the surface radiation effect on the natural convection in differentially heated square cavities with isothermal side walls and adiabatic horizontal walls. In various applications encountered in solar technology, such as solar receivers, the wall temperature is not uniform; instead, the temperature is variable as a consequence of the heat flux imposed on its side. Depending on the density of heat flux from the side with zero wall thickness and on geometrical and thermal conditions of a wall with finite thickness and conductivity, various interactions between convection—conduction and radiation will result. Our aim in this study is to determine the effect of the surface radiation on the conjugate heat transfer by natural convection and conduction in an inclined enclosure having two active sides and the two others insulated. One of the active sides is subject to a constant heat flux and the other one with finite wall thickness and conductivity. We would also study the effect of the other parameters such as wall thickness, its conductivity and the inclination of the enclosure on the convective and radiative heat transfer.

2. Problem description and mathematical model

The system to study is shown in Fig. 1. It is an enclosure bounded on the right by a massive wall with a finite wall thickness and conductivity. We impose a constant heat flux on the left active wall to simulate solar radiation input and a constant

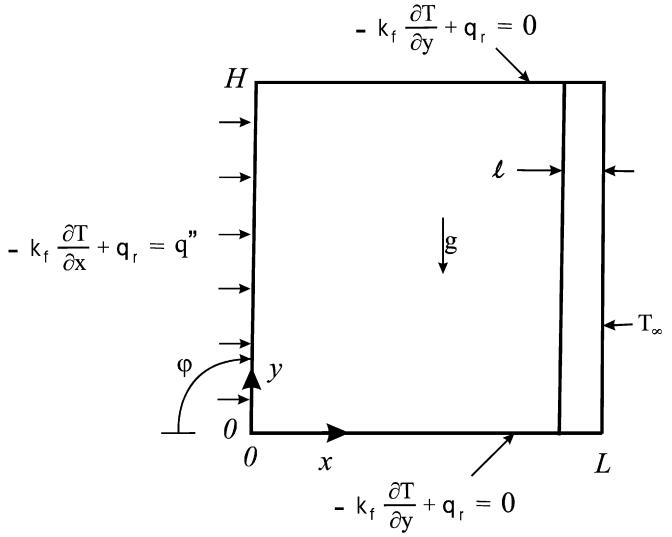

Fig. 1. Schematic of square enclosure bounded by a solid wall, the coordinate system and boundary conditions.

temperature on the right outer boundary of the wall to simulate uniform fluid temperature at the adjoining space. The horizontal boundaries are adiabatic. Boundary conditions are shown in Fig. 1.

2.1. Convection and conduction formulation

We assume that the fluid is Newtonian, and the third dimension has a negligible effect on the flow and heat transfer. With these assumptions, we use two-dimensional conservation equations for mass, momentum and energy with Boussinesq approximation. By using H as the length scale, α_f/H as the velocity scale, Hq''/k as the temperature scale, $\rho\alpha_f^2/H^2$ as the pressure scale and H^2/α_f as the time scale, we obtain following non-dimensional equations

$$\frac{\partial U}{\partial X}+\frac{\partial V}{\partial Y}=0 \tag{1}$$

$$\frac{\partial U}{\partial \tau}+U\frac{\partial U}{\partial X}+V\frac{\partial U}{\partial Y} =-\frac{\partial P}{\partial X}+\Gamma Pr\nabla^2 U+Ra\,Pr\theta\cos\varphi \tag{2}$$

$$\frac{\partial V}{\partial \tau}+U\frac{\partial V}{\partial X}+V\frac{\partial V}{\partial Y} =-\frac{\partial P}{\partial Y}+\Gamma Pr\nabla^2 V+Ra\,Pr\theta\sin\varphi \tag{3}$$

$$\frac{\partial \theta}{\partial \tau}+U\frac{\partial \theta}{\partial X}+V\frac{\partial \theta}{\partial Y}=\alpha_r\nabla^2\theta \tag{4}$$

We note that to obtain steady state solutions, we are using unsteady state equations for better convergence in the numerical computation. Γ in Eqs. (2) and (3) is a general diffusion coefficient, which is equal to 1 in the fluid region and 10^{15} in the solid region; it is introduced to ensure that $U=V=0$ everywhere including at the solid–fluid interface. α_r in Eq. (4) is the ratio of the thermal diffusivities α_s/α_f and it is equal to 1 in the fluid region and α_s/α_f in the solid region. In numerical simulation at each time step, we have to satisfy the energy conservation at the interface between the solid and the fluid, i.e. in the X direction, for example, $k_s\partial\theta_s/\partial X=k_f\partial\theta_f/\partial X$ or $k_r\partial\theta_s/\partial X=\partial\theta_f/\partial X$ with $k_r=k_s/k_f$. For the steady state solution, we have $\alpha_r\nabla^2\theta=0$ which becomes $k_r\nabla^2\theta=0$; thus, we have to specify only the conductivity ratio, k_r for the steady state solution of the problem.

2.2. Radiation formulation

We assume that the walls are diffuse and grey, and the air is a non-absorbing medium. For an area on a surface, the non-dimensional energy conservation equation is [13]

$$\sum_{j=1}^{N}(\delta_{ij}-F_{ij})\sigma T_j^4=\sum_{j=1}^{N}\left[\delta_{ij}-(1-\varepsilon_j)F_{ij}\right]\frac{q_j}{\varepsilon_j} \tag{5a}$$

where

$$\delta_{ij}=\begin{cases}1, & \text{if } i=j\\ 0, & \text{if } i\neq j\end{cases}\quad\text{and}\quad q_j=Q_j/A_j.$$

Using the definitions of $\Theta=T_i/T_\infty$ and $\zeta_i=q_i/\sigma T_\infty^4$ we obtain

$$\sum_{j=1}^{n}(\delta_{ij}-F_{ij})\Theta_j^4=\sum_{j=1}^{n}\left[\delta_{ij}-(1-\varepsilon_j)F_{ij}\right]\frac{\zeta_j}{\varepsilon_j} \tag{5b}$$

At the surface:

$$N_r\zeta=\left(\frac{\partial\theta_f}{\partial X}-k_r\frac{\partial\theta_s}{\partial X}\right) \tag{6}$$

where $N_r=\sigma T_\infty^4/q''$ is the radiation number, $\partial\theta_f/\partial X$ and $\partial\theta_s/\partial X$ are the heat flux from the wall surface to the fluid on the right and to the solid on the left, respectively.

The governing parameters are $Ra=g\beta q''H^4/(\upsilon\alpha k)$, $Pr=\upsilon/\alpha$, k_r, ε, and $A=L/H$ and $w=l/H$.

The average convective and radiative Nusselt numbers are calculated at $X=0$ plane as

$$Nu_c=-\int_0^1\frac{1}{\theta}\frac{\partial\theta}{\partial X}\,dY \tag{7}$$

$$Nu_r=\int_0^1\frac{1}{\theta}N_r\zeta_s\,dY \tag{8}$$

The stream function is calculated from its definition as

$$U=-\frac{\partial\psi}{\partial Y},\qquad V=\frac{\partial\psi}{\partial X} \tag{9}$$

ψ is zero on the solid surfaces and the streamlines are drawn by $\Delta\psi=(\psi_{\max}-\psi_{\min})/n$ with n is the number of increments.

Boundary conditions are

On solid surfaces:

$$U=0,\qquad V=0 \tag{10}$$

Table 1
Validation study of natural convection and conduction in a square enclosure [6]

		[6]				This study			
	Ra	10^3	10^4	10^5	10^6	10^3	10^4	10^5	10^6
$k_r = 5$	*Nu*	1.070	1.720	2.850	4.650	1.054	1.803	2.988	4.586
$k_r = 10$	*Nu*	1.070	1.720	2.950	4.910	1.068	1.806	2.975	4.979

$X = 0$ to $A - w$, at $Y = 0$ and 1:

$$-\frac{\partial\theta}{\partial Y} + N_r\zeta = 0 \tag{11a}$$

$X = A - w$ to A, $Y = 0$ and 1:

$$\frac{\partial\theta}{\partial Y} = 0 \tag{11b}$$

$X = 0$, $Y = 0$ to 1:

$$q = -\frac{\partial\theta}{\partial X} + N_r\zeta = 1 \tag{12}$$

$X = A$, $Y = 0$ to 1:

$$\theta = 0 \tag{13}$$

3. Numerical technique

The numerical method used to solve Eqs. (1) to (6) with the boundary conditions Eqs. (10) to (13) is the SIMPLER (Semi-Implicit Method for Pressure Linked Equations Revised) algorithm [14]. The computer code based on the mathematical formulation presented above and the SIMPLER method were validated with the benchmark [15]. The results showed that the deviations in Nusselt number and the maximum stream function at $Ra = 10^5$ were 1.84% and 0.97%, respectively. Similarly at $Ra = 10^6$, they were 1.74% and 1.09%, respectively. It was seen that the concordance was excellent. In addition, the average Nusselt numbers at the hot and cold walls were compared, which showed a maximum difference of about 0.5% in all runs. The present code was tested also to simulate the case of conjugate heat transfer by conduction and convection in enclosures bounded by a solid wall [6]. The results are presented in Table 1, which shows an excellent agreement. Additionally, we simulated the case of conjugate heat transfer by convection, conduction and radiation in a partitioned square enclosure [11]. The results are presented in Table 2, which shows good agreements.

Non-uniform grid in X and Y direction was used for all computations. Grid convergence was studied for the case of square cavity having $w = 0.05$ and $k_r = 20$ with grid sizes from 35×30 to 85×80 at $Ra = 10^9$. The results are presented in Table 3. We see that for grid sizes of 55×50 and 85×80, the variation in convective Nusselt number is 0.15%, in radiative Nusselt number it is 4.95% and in radiative heat flux 0.07%. Thus, 55×50 grid size was a good choice from the computation time and precision point of view for the square cavity. The grid size in the wall was 5 in the X direction for all cases and the rest were in the cavity. We obtained similar results at $Ra = 3 \times 10^{10}$ as can be seen in Table 3. Using a computer with a dual processor of 1.83 GHz clock speed, for $A = 1$, with 55×50 grid size, at $Ra = 10^9$, the typical execution time was 36 s and at $Ra = 10^{10}$, it was 80 s. We carried out tests to obtain the most favourable relaxation coefficient for converged solutions. We varied the relaxation coefficient of temperature and found that 0.5 was satisfactory to obtain converged solution with reasonable computation times. A similar study showed the relaxation coefficient of 0.1 produced stable solutions for velocity field.

Table 2
Validation study of natural convection, conduction and radiation in a square partitioned enclosure

			[11]			This study		
		Ra	10^6	10^7	10^8	10^6	10^7	10^8
w	0.025	*Nu*	11.00	17.00	29.00	11.19	17.81	29.03
	0.050		12.80	21.50	31.00	12.61	21.80	31.43
	0.100		13.60	21.50	31.00	13.78	22.32	31.43
	0.150		14.10	21.50	31.00	13.67	21.98	30.97
	0.200		15.00	21.50	31.00	14.61	22.95	31.58
w	0.025	$\dot{V}$	3.00	14.00	39.00	3.17	14.51	40.33
	0.050		8.00	25.00	50.00	8.23	25.27	50.88
	0.100		12.50	29.00	49.00	12.15	30.72	53.46
	0.150		13.15	30.00	50.00	12.72	29.62	49.37
	0.200		13.90	30.00	50.00	13.76	31.53	53.72

Table 3
Grid independence study at $Ra = 10^9$ and 3×10^{10} with $A = 1$, $w = 0.10$, $k_r = 20$, $\varphi = 90°$

Ra	Size	Nu_c	%	Nu_r	%	q_r/q_t	%	Exec *t* (s)
1×10^9	35×30	14.344	*1.76*	22.703	*16.89*	0.889	*0.45*	17
	45×40	14.100	*0.03*	21.289	*9.61*	0.891	*0.15*	26
	55×50	14.075	*0.15*	20.383	*4.95*	0.892	*0.07*	36
	65×60	14.025	*0.50*	19.955	*2.75*	0.893	*0.00*	51
	75×70	14.058	*0.27*	19.590	*0.87*	0.893	*0.00*	68
	85×80	14.096	*0.00*	19.421	*0.00*	0.893	*0.00*	89
3×10^{10}	35×30	29.330	*0.88*	20.024	*11.25*	0.768	*2.08*	66
	45×40	29.839	*0.84*	18.948	*5.28*	0.769	*1.85*	95
	55×50	30.067	*1.61*	18.709	*3.95*	0.773	*1.40*	80
	65×60	29.613	*0.08*	18.251	*1.40*	0.779	*0.59*	104
	75×70	29.544	*0.16*	18.241	*1.35*	0.784	*0.03*	121
	85×80	29.590	*0.00*	17.998	*0.00*	0.784	*0.00*	162

A converged steady state solution was obtained by iterating in time until variations in the primitive variables between subsequent time steps were:

$$\sum\left|\left(\varphi_{i,j}^{\text{old}} - \varphi_{i,j}\right)\right| < 10^{-4} \tag{14}$$

where φ stands for U, V, and θ.

Within the same time step, the residual of the pressure term was less than 10^{-3} [14]. In addition, the accuracy of the solution was double-checked using the energy conservation on the domain to ensure it was less than 10^{-4}.

4. Results and discussion

The aspect ratio is constant $A = 1$. The variable geometrical parameter is the dimensionless wall thickness, $w = 0.0$, 0.05, 0.10 and 0.15. The Rayleigh number is varied from $Ra = 10^8$ to 3×10^{10}. The Prandtl number, $Pr = 0.70$ for air is kept constant.

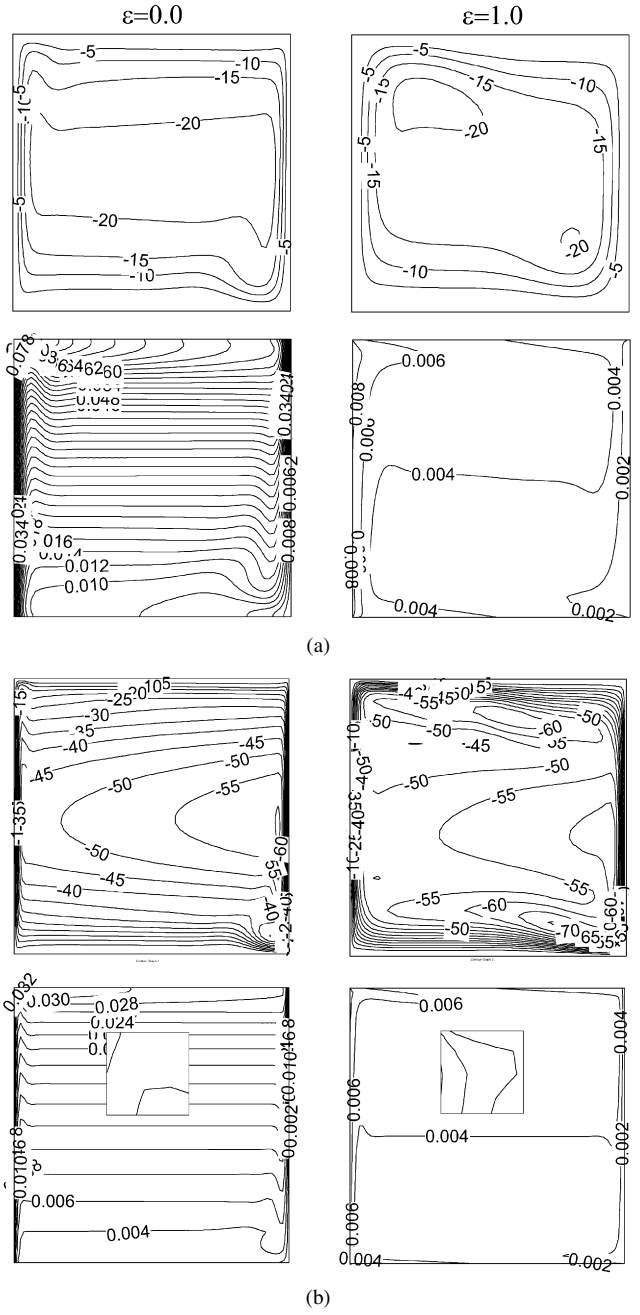

Fig. 2. Streamlines and isotherms for $A = 1$, $w = 0.0$, $\varphi = 90°$ and $\varepsilon = 0.0$ and 1.0. (a) $Ra = 10^8$, (b) $Ra = 10^{10}$. Streamlines are shown in the first row and the isotherms in the second for each case. The inserts in (b) are the enlarged isotherms at the left upper corner of the enclosure.

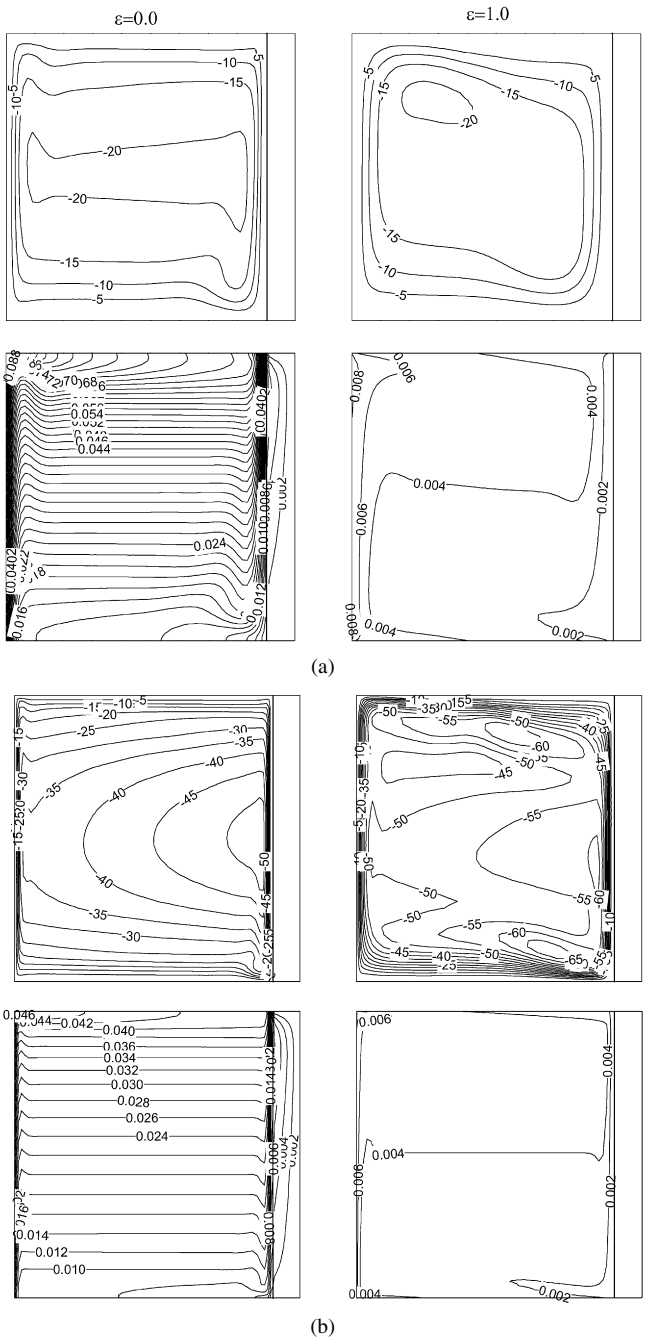

Fig. 3. Streamlines and isotherms for $A = 1$, $w = 0.10$, $\varphi = 90°$, $k_r = 20$ and $\varepsilon = 0.0$ and 1.0. (a) $Ra = 10^8$, (b) $Ra = 10^{10}$. Streamlines are shown in the first row and the isotherms in the second for each case.

The conductivity ratio is varied from $k_r = 10$, 20 and 40, which are representative of materials like silica, Teflon and glass, respectively. The inclination angle φ is varied from 60 to 180° with $\varphi = 90°$ for horizontal position. We will present first the results for the case with $A = 1$ and $\varphi = 90°$, and then the effect of φ on the results. We will be using the Rayleigh number, $Ra = g\beta q'' H^4 / k\alpha_f \nu$ to present both Nu_c and Nu_r computed at $X = 0$ plane by Eqs. (7) and (8), respectively, and the combined Nusselt number, Nu_t.

For the simulation of the system shown in Fig. 1, we specified $H = 0.727$ m, $T_\infty = 300$ K. We had the following range for the radiation number: $4592.7 > N_r > 15.3$ at Ra from 10^8 to 3×10^{10}, respectively; i.e. N_r is a decreasing function of Ra.

4.1. Flow patterns and isotherms

We will examine the influence of the surface radiation on the flow and temperature fields for the case of $A = 1$, $w = 0$ and 0.10, $\varepsilon = 0$ and 1, $k_r = 20$ and $Ra = 10^8$ and 10^{10}. We present the case with $w = 0$ in Fig. 2 and with $w = 0.10$ in Fig. 3. The flow pattern and isotherms for the surface emissivity $\varepsilon = 0$ are shown in the first column and for $\varepsilon = 1$ in the second

of Figs. 2 and 3. We note also that for a fair comparison, we kept the increment of $\Delta\Psi = 5$ for streamlines and $\Delta\theta = 2 \times 10^{-3}$ for isotherms in all iso-figures except the inserted figures in Fig. 2(b). The latter was set at $\Delta\theta = 1 \times 10^{-2}$ for $\varepsilon = 0$ and 1×10^{-3} for $\varepsilon = 1$ to differentiate the isotherms at the upper corner.

For the case with $w = 0$ at $Ra = 10^8$ in Fig. 2(a), the streamlines for $\varepsilon = 0$ show a stratified and boundary layer flow on the left and right boundaries. For $\varepsilon = 1$, the flow field is completely modified though the circulation strength is a little less than that for $\varepsilon = 0$. Indeed, Ψ_{ext} for $\varepsilon = 0$ is -23.23 ($X = 0.9133$, $Y = 0.475$) and for $\varepsilon = 1$ it is -21.55 ($X = 0.2897$, $Y = 0.766$). We see that the extremum is shifted upward and a second circulation is present at the lower right part. The isotherms complement the observation about streamlines. The equally distanced isotherms show that the temperature field for $\varepsilon = 0$ is intense and the temperature gradients are large at the active walls and they are small and reduced by an order of magnitude for $\varepsilon = 1$. In Fig. 2(b), at $Ra = 10^{10}$ the circulation is enhanced; Ψ_{ext} for $\varepsilon = 0$ is -60.91 ($X = 0.9593$, $Y = 0.452$) and for $\varepsilon = 1$ it is -70.74 ($X = 0.7757$, $Y = 0.100$). The circulation for $\varepsilon = 1$ is increased with respect to that for $\varepsilon = 0$ and there are multiple cells formed. We note that high velocity gradients are equally present on horizontal adiabatic boundaries; the strength of circulation in this case is increased by 16% with the surface radiation. Additionally, at the corners of the left active wall, the circulation is more intensive than that for $\varepsilon = 0$. The isotherms for $\varepsilon = 0$ show that the pattern described in (a) is the same but weakened with lower temperature gradients in the boundary layer flow. For $\varepsilon = 1$, the temperature field is similar to that in (a) but the gradients are much higher than those for $Ra = 10^8$. However comparing the cases with $\varepsilon = 0$ and $\varepsilon = 1$ we see that generally the temperature field is more intense and the gradients much higher for $\varepsilon = 0$ than $\varepsilon = 1$. Thus, despite increased strength of circulation, it is expected that the convective heat transfer be decreased with surface radiation. To differentiate better, we reproduced the isotherms at the upper corner with $\Delta\theta = 10^{-2}$ for $\varepsilon = 0$ and $\Delta\theta = 10^{-3}$ for $\varepsilon = 1$ and shown as inserts in Fig. 2(b). We note the high temperature gradients for $\varepsilon = 1$ near the corner despite generally lower gradients elsewhere; we will discuss it later when presenting local temperature and the local Nusselt number on the left active wall.

For the case with $w = 0.10$ at $Ra = 10^8$ in Fig. 3(a), the streamlines for $\varepsilon = 0$ show a similar stratified and boundary layer flow to that with $w = 0$, though the strength of circulation is decreased due to the wall thermal resistance; Ψ_{ext} for this case is -21.52 ($X = 0.8098$, $Y = 0.475$) and the strength of the circulation is decreased by 7.4% with respect to that in Fig. 2(a). The appearance of isotherms is almost the same as with $w = 0$, although the intensity of the temperature field is increased slightly. Obviously this is an indication of reduced convection due to the presence of the wall. For $\varepsilon = 1$, the flow and temperature fields look similar to those with $w = 0$. In comparison with the $\varepsilon = 0$ case, the strength of circulation is slightly decreased with $\Psi_{\text{ext}} = -21.11$ ($X = 0.2960$, $Y = 0.766$). At $Ra = 10^{10}$ in Fig. 3(b), for $\varepsilon = 0$, we have the flow and temperature fields similar to those $w = 0$ but the circulation strength is reduced by 12.3% and the temperature gradients increased. For this case $\Psi_{\text{ext}} = -53.39$ ($X = 0.8574$, $Y = 0.475$). For $\varepsilon = 1$, the flow and temperature fields are slightly modified with increasing Rayleigh number, however the pattern is the same. The strength of circulation $\Psi_{\text{ext}} = -68.33$ ($X = 0.6906$, $Y = 0.101$) is higher due to the presence of the wall. Again we observe multiple cells, a complete boundary layer flow on all four surfaces and with low velocity and temperature gradients. In this case the strength of circulation is increased by 28% with respect to that with $\varepsilon = 0$. Lower temperature gradients with surface radiation are an indication that the convective heat transfer will be lower despite increased circulation strength with multiple cells. In the case of surface radiation, the increase of the circulation strength may be due to the fact that we have heat transfer by convection at all four surfaces resulting in a chaotic multi-cellular pattern however with lower temperature gradients at the active walls.

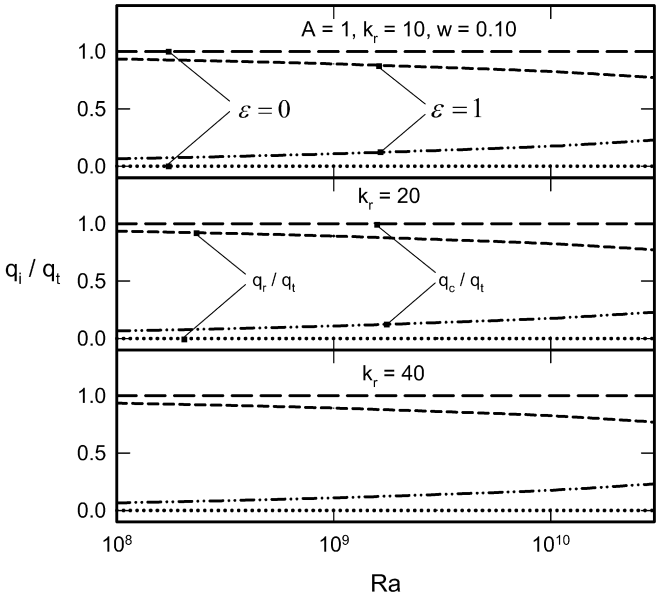

Fig. 4. Dimensionless heat fluxes by convection and radiation as a function of the Rayleigh number for the case of $A = 1$, $w = 0.10$, $\varphi = 90°$, and $\varepsilon = 0.0$ and 1.0 with k_r variable from 10 to 40.

4.2. Heat transfer

The conjugate heat transfer is by convection and radiation through the cavity, the combined heat flux, $q_t = q''$ is the sum of the heat fluxes, q_c, q_r which is transferred by conduction through the wall. Hence

$$\frac{q_c}{q_t} + \frac{q_r}{q_t} = 1 \tag{15}$$

For the case with $A = 1$, $w = 0.10$ and $\varepsilon = 0$ and 1 with k_r as a parameter, we present q_i/q_t (i takes c and r) as a function of the Rayleigh number in Fig. 4. We see for all k_r that with $\varepsilon = 0$, i.e. no radiation exchange, $q_r/q_t = 0$ and $q_c/q_t = 1$. With $\varepsilon = 1$, the radiative heat flux is much higher than the convective heat flux, and q_r/q_t is a decreasing function of Ra while q_c/q_t is an increasing function of it. As expected, the variations

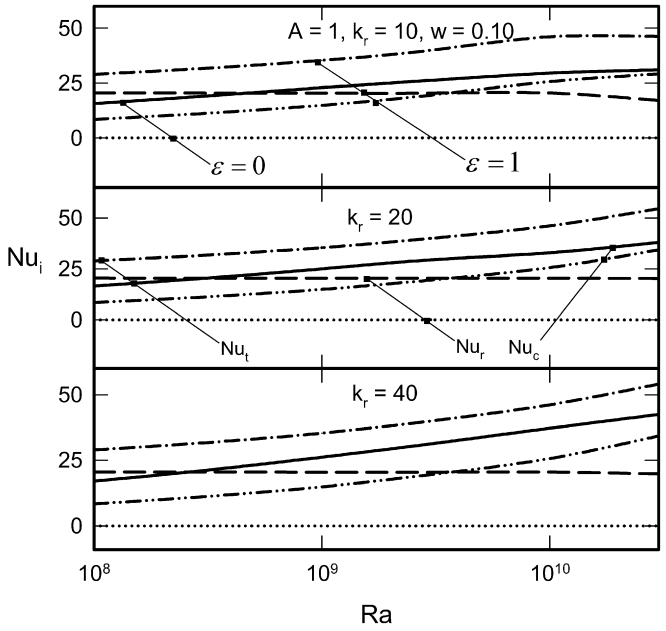

Fig. 5. Convective, radiative and combined Nusselt numbers as a function of the Rayleigh number. $A = 1$, $w = 0.10$, $\varphi = 90°$, and $\varepsilon = 0.0$ and 1.0 with k_r is variable from 10 to 40.

of q_c/q_t and q_r/q_t are independent of the conductivity ratio, k_r since the sum of the two in Eq. (15) is always equal to 1 and constant, and $q_c/q_t = 1$ regardless of the Rayleigh number. The same data plotted as Nu_i as a function of Ra presented in Fig. 5 show that convective and radiative Nusselt numbers have the same order of magnitude. Nu_r is slightly decreasing function of Ra while Nu_c is an increasing function of it. Further, we note that although Nu_r is quasi-independent of the conductivity ratio, Nu_c is an increasing function of it. As a result, Nu_t is an increasing function of the Rayleigh number. These observations in Figs. 4 and 5 are expected since the radiation number is a decreasing function of the Rayleigh number as stated earlier at the first paragraph of Section 4. As a result, we have Nu_r is slightly increasing function of N_r and decreasing function of Ra. In consequence, Nu_c is a strong decreasing function of N_r and an increasing function of Ra. The combined Nusselt number Nu_t is a strongly decreasing function of N_r and as a result, it is an increasing function of Ra.

For the case with $A = 1$, $w = 0.10$ and $k_r = 20$ with Ra from 10^8 to 10^{10}, we plotted q_i/q_t as a function of ε from zero to one in Fig. 6(a). We observe that q_r/q_t is a strong increasing function of ε and q_c/q_t is a decreasing function of it. The variation is strong with ε increasing from zero up to $\varepsilon = 0.6$ thereafter weak. The Nusselt numbers, Nu_c, Nu_r and Nu_t as a function of ε for the same case are presented in Fig. 6(b). As expected from q_i/q_t versus ε results in Fig. 6(a), the radiative Nusselt number is an increasing function of the surface emissivity and the convective Nusselt number is a decreasing function of it. Since the radiative Nusselt number is a strong increasing function of ε, the combined Nusselt number is also an increasing function of it.

The influence of surface radiation on the temperature, θ and the local convection Nusselt number, Nu_{loc} along the boundary

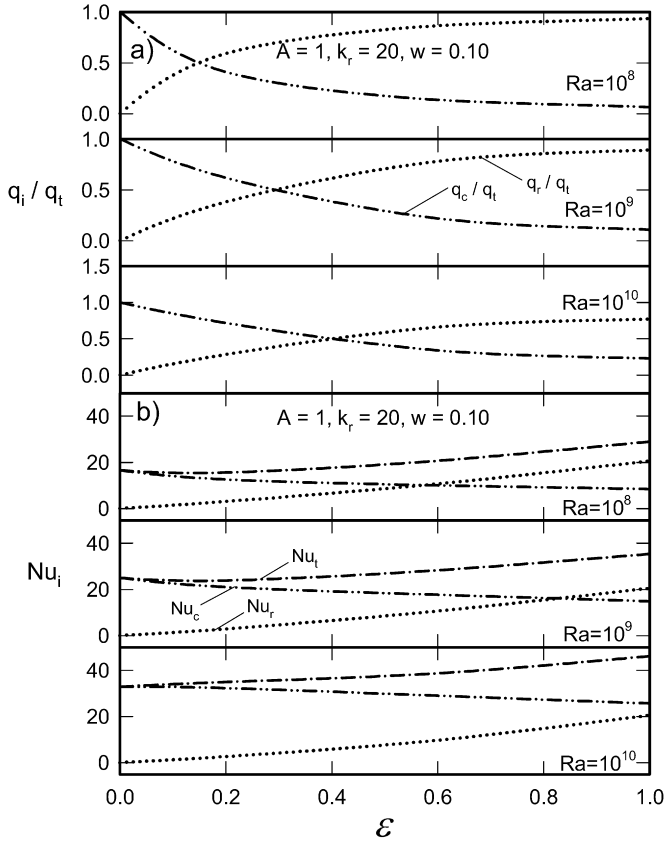

Fig. 6. For the case of $A = 1$, $w = 0.10$, $\varphi = 90°$, $k_r = 20$ and Ra from 10^8 to 10^{10}, (a) dimensionless heat fluxes by convection and radiation as a function of the surface emissivity, (b) convective, radiative and combined Nusselt numbers as a function of the surface emissivity.

at $X = 0$ is presented in Fig. 7; the temperature is presented on the left side and the local Nusselt number on the right for the case of $A = 1$, $w = 0.10$, $\varphi = 90°$ and $k_r = 20$ with $Ra = 10^{10}$. We see in Fig. 7 that for $\varepsilon = 0$, i.e. no surface radiation, the variation of the temperature is non-linear and for $\varepsilon = 1$, it is almost constant. These results are expected since for $\varepsilon = 0$, the cooling is better at the lower parts of the wall because the incoming air is cooler; then, as the air heated along the wall, the cooling becomes less effective as a result of which the wall temperature increases. For $\varepsilon = 1$, due to radiative exchange among the walls, the wall temperature is almost constant with slight increase of the wall temperature at the upper part. Thus, the influence of surface radiation is far from negligible as it changes the temperatures on the enclosure walls, including the adiabatic ones. In a way, the radiation heat exchange plays the role of making the active wall temperature quasi-uniform. For the same case, the variation of the local Nusselt number on the right-hand side of Fig. 7 is non-linear for $\varepsilon = 0$, higher at the bottom of the enclosure, lower at the top, which is a consequence of the variation of the temperature discussed above. This is expected since the convective heat transfer is higher for cooler fluid sweeping the hot vertical wall than that of warmer fluid doing the same at the top. The variation of the local Nusselt number is modified for $\varepsilon = 1$ in such a way to have a high local Nusselt number at the bottom and top of the active wall, and reduced values in be-

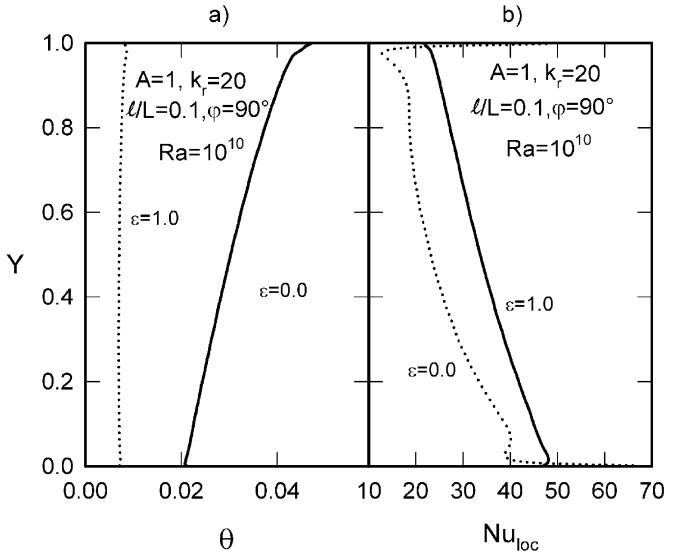

Fig. 7. For the case of $A = 1$, $w = 0.10$, $\varphi = 90°$, $k_r = 20$ and $Ra = 10^{10}$, the temperature at $X = 0$ along the wall for $\varepsilon = 0.0$ and 1.0 on the left side of the figure and the local convective Nusselt number at $X = 0$ along the wall for $\varepsilon = 0.0$ and 1.0 on the right.

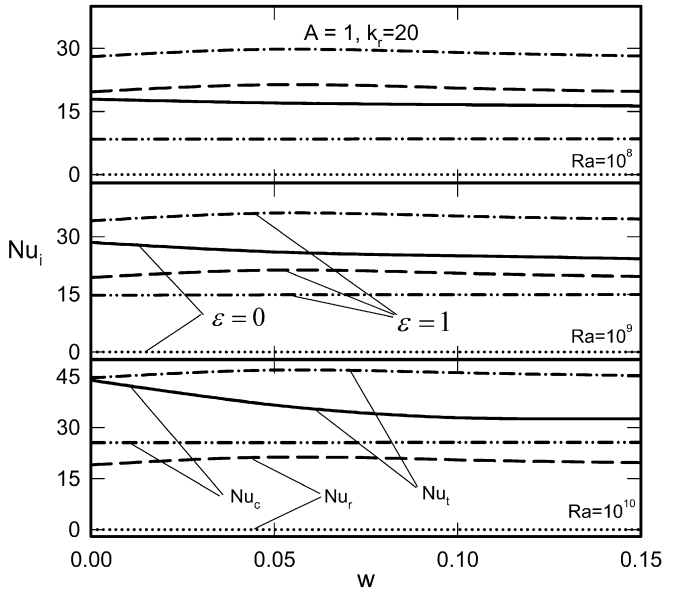

Fig. 8. Convective, radiative and combined Nusselt numbers as a function of the wall thickness for the case of $A = 1$, $\varphi = 90°$, $k_r = 20$, $\varepsilon = 0.0$ and 1.0, and Ra from 10^8 to 10^{10}.

tween than those for $\varepsilon = 0$. These representative results confirm our observations of the flow and temperature fields discussed earlier with Figs. 2 and 3. Indeed, in the inserts of Fig. 2(b), we note higher temperature gradients near the corner with $\varepsilon = 1$ than those with $\varepsilon = 0$ with isotherms bending towards the corner instead of following the horizontal boundary. The reason for the increased temperature gradients is due to radiative heat exchange between the insulated walls and the active vertical walls. This pattern near the corners with surface radiation has also been observed by Akiyama and Chong [7].

We noted earlier in Fig. 4 that q_i/q_t is independent of the wall thickness, w. Indeed, a plot of q_i/q_t as a function of w

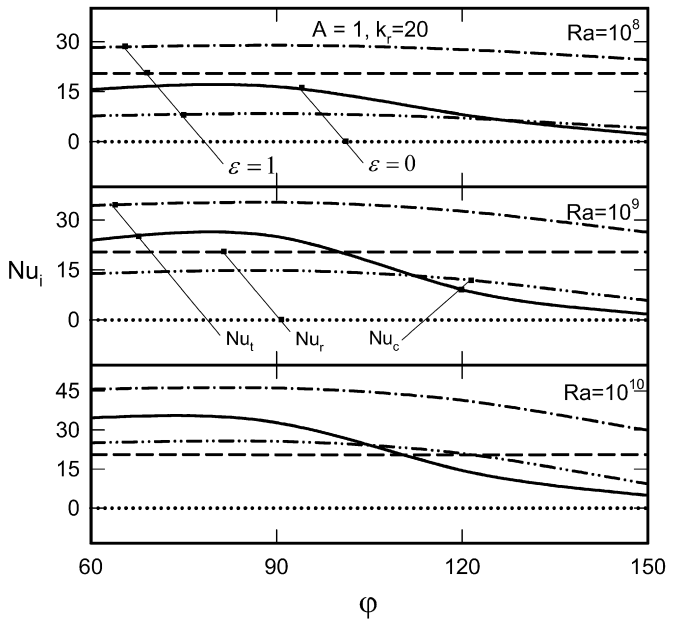

Fig. 9. Convective, radiative and combined Nusselt numbers as a function of the enclosure inclination angle for the case of $A = 1$, $k_r = 20$, $\varepsilon = 0.0$ and 1.0, and Ra from 10^8 to 10^{10}.

with $A = 1$, $k_r = 20$, $\varepsilon = 0$ and 1 and Ra from 10^8 to 10^{10} showed that this was the case (not shown here). The same data plotted as Nu_i as a function of w is presented in Fig. 8. For $\varepsilon = 0$, the convective Nusselt number is an increasing function of the Rayleigh number and a decreasing function of the wall thickness. The latter is expected since the wall conductance decreases with increasing wall thickness. For $\varepsilon = 1$, at $Ra = 10^8$ and 10^9, Nu_r is slightly greater than Nu_c and at $Ra = 10^{10}$, Nu_r is slightly smaller than Nu_c. It appears also that the combined Nusselt number, Nu_t goes through a broad maximum at about $w = 0.05$.

4.3. Effect of the inclination angle

We present in Fig. 9 the convective, radiative and combined Nusselt numbers as a function of the inclination angle, φ for the case of $A = 1$, $k_r = 20$, $\varepsilon = 0$ and 1 with $Ra = 10^8$, 10^9 and 10^{10}. We observe that for $\varepsilon = 0$, the radiative Nusselt number is zero and $Nu_c = Nu_t$ at all Rayleigh numbers Further, Nu_c is an increasing function of Ra and at each Rayleigh number, it goes through a maximum at φ about 80°. For $\varepsilon = 1$, Nu_r is quasi-constant and equal to about 20.5 at all Rayleigh numbers, Nu_c is a decreasing function of φ, especially at high inclination angles. The observed quasi-constancy of the radiative Nusselt number is due to the fact that at a given Rayleigh number, i.e. at a corresponding radiation number, we found that the radiative heat flux q_r/q_t was increased with the inclination angle φ. This is expected because the convective heat flux q_c/q_t is a decreasing function of the inclination angle and following equation (15), the radiative heat flux should increase. At the same condition, the average wall temperature $\theta_{X=0}$ was also increased with the inclination angle φ at the same rate as that of q_r/q_t. Indeed we observed for $Ra = 10^{10}$ for example that both q_r/q_t and

$\theta_{X=0}$ was quasi-constant for φ from 60 to 90°, thereafter they increased by 12.5% from 90 to 150°. The Nusselt number being proportional to the heat flux divided by the temperature, we found that the radiative Nusselt number Nu_r is quasi-constant as presented in Fig. 9. The reason for the observed variation of Nu_c with the inclination angle will be visualized and explained later in Fig. 10. The contribution of Nu_r is larger than that of Nu_c at $Ra = 10^8$ and 10^9. At $Ra = 10^{10}$ however, the contribution of Nu_c is greater than that of Nu_r for φ up to 120°, thereafter it reverses. The overall result is that due to the influence of surface radiation, the convective Nusselt number is increased for low inclination angle and decreased at high inclination angle, and the combined Nusselt number, Nu_t is greatly increased due to contribution of Nu_r. For example, at $Ra = 10^{10}$, the increase in Nu_t with respect to that with $\varepsilon = 0$ is about 31.8% at $\varphi = 60°$ and 51.5% at $\varphi = 150°$.

To see the influence of surface radiation on the flow and temperature fields at different inclination angles, we present for the case of $A = 1$, $k_r = 20$, $\varepsilon = 0$ and 1 at $Ra = 10^{10}$, streamlines and isotherms for $\varphi = 60$, 120 and 150° in Fig. 10 (a)–(c), respectively. The first row in each case is the flow field and the second is the temperature field. Isolines are traced with $\Delta\Psi = 5$ and $\Delta\theta = 0.01$ for $\varepsilon = 0$ and 0.001 for $\varepsilon = 1$ and to prevent cluttering, the labels are shown only for the case of $\varphi = 120°$ Fig. 10(b). We see in Fig. 10 (a)–(c) that for $\varepsilon = 0$ and 1, the isotherms showing stratification in the enclosure are almost perpendicular to the vertical and the flow and temperature fields are also modified accordingly. The influence of surface radiation on the flow field in each case is to make the velocity gradients significant on all four boundaries. The strength of circulation is reduced with increasing φ for both $\varepsilon = 0$ and 1. For $\varepsilon = 0$, Ψ_{ext} is -104.4252, -21.4525 and -10.5591 for $\varphi = 60$, 120 and 150°, respectively; for $\varepsilon = 1$, it is -113.0185, -40.4129 and -21.4166. We see also that the strength of the circulation is increased considerably with surface radiation, especially for higher inclination angles. However, we see that the flow fields became multi-cellular and the temperature gradient is decreased, which is consistent with the heat transfer results of Fig. 9.

5. Conclusion

We studied conjugate heat transfer by natural convection, conduction and radiation in inclined square cavities boarded by a solid wall with finite conductivity. The constant heat flux is imposed on one of the active walls, the other being at isothermal condition. The other two boundaries are adiabatic. The aspect ratio is 1 and constant and the wall thickness is varied from 0.0 to 0.15. The Rayleigh number is varied from 10^8 to 3×10^{10}, the conductivity ratio from 10 to 40; the Prandtl number is 0.7. Coupled conservation equations of mass, momentum and energy were solved by finite difference method using SIMPLER algorithm. In view of the results presented, the main points can be summarized as follows.

The surface radiation modifies the flow and temperature fields. In particular, the temperatures on all enclosure walls are modified; the velocity and temperature gradients are decreased.

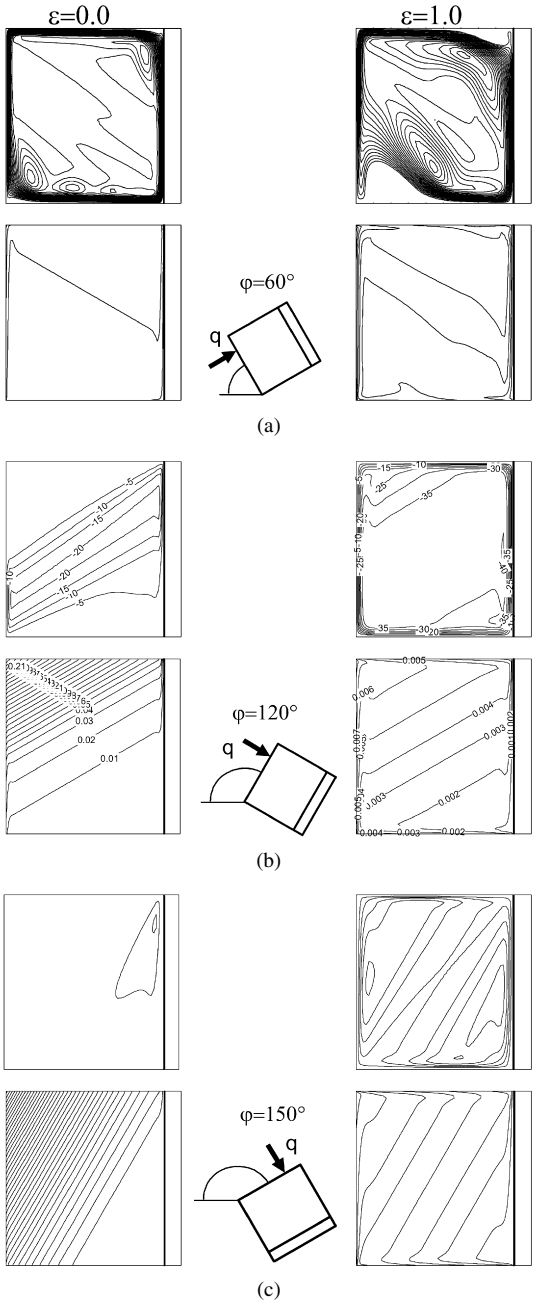

Fig. 10. Streamlines and isotherms for (a) $\varphi = 60°$, (b) $\varphi = 120°$ and (c) $\varphi = 150°$ for the case of $A = 1$, $w = 0.10$, $k_r = 20$, $\varepsilon = 0.0$ and 1.0 and $Ra = 10^{10}$. For each case, streamlines are shown in the first row and the isotherms in the second.

The contribution of the surface radiation heat flux is more important than that of the natural convection at all Rayleigh numbers. Heat flux by natural convection increases gradually with increasing Rayleigh number, as a consequence of which that by radiation decreases gradually with it. The radiative heat flux is a strong increasing function of the surface emissivity starting at its low values; as a consequence, the convective heat flux is a strongly decreasing function of it.

The convective Nusselt number Nu_c is an increasing function of the Rayleigh number Ra and the radiative Nusselt number Nu_r is insensitive to its variation. As a result the combined

Nusselt number Nu_t is an increasing function of Ra. The convective Nusselt number Nu_c decreases slightly with increasing surface emissivity ε; thus, the effect of the surface radiation on the convective Nusselt number is not as strong as that of the Rayleigh number. The radiative Nusselt number Nu_r, on the other hand, is an increasing function of the surface emissivity, ε. The convective and radiative Nusselt numbers have the same order of magnitude and generally, the combined Nusselt number Nu_t is an increasing function of ε. The influence of conductivity ratio and wall thickness on the Nusselt numbers is not significant; however Nu_r as well as Nu_t are slightly increasing function of the wall thickness at its small values. The convective Nusselt number Nu_c goes through a broad maximum at the inclination angle of about 80° while the radiative Nusselt number Nu_r is not sensitive to its variation.

Acknowledgement

The financial support for this study by Natural Sciences and Engineering Research Council Canada is acknowledged.

References

[1] E. Bilgen, J. Michel, Integration of solar systems in architectural and urban design, in: A.A.M. Sayigh (Ed.), Solar Energy Application in Buildings, Academic Press, 1979 (Chapter 19).

[2] A.E. Bergles (Ed.), Heat Transfer in Electronic and Microelectronic Equipment, Hemisphere Publishing Corp., New York, 1990.

[3] C. Prakash, D.A. Kaminski, Conjugate natural convection in square enclosure: Effect of conduction in one of the vertical walls, HTD ASME 39 (1984) 49–54.

[4] Z.-G. Du, E. Bilgen, Coupling of wall conduction with natural convection in a rectangular enclosure, Int. J. Heat Mass Transfer 35 (1992) 1969–1975.

[5] M. Mbaye, E. Bilgen, P. Vasseur, Natural convection heat transfer in an inclined porous layer boarded by a finite thickness wall, Int. J. Heat Fluid Flow 14 (1993) 284–291.

[6] R. Ben Yedder, E. Bilgen, Natural convection in inclined enclosures bounded by a solid wall, Heat Mass Transfer 32 (1997) 455–462.

[7] M. Akiyama, Q.P. Chong, Numerical analysis of natural convection with surface radiation in a square cavity, Numer. Heat Transfer Part A 31 (1997) 419–433.

[8] N. Ramesh, S.P. Venkateshan, Effect of surface radiation on natural convection in a square enclosure, J. Thermophys. Heat Transfer 13 (3) (1999) 299–301.

[9] S. Balaji, S.P. Venkateshan, Interaction of surface radiation with free convection in a square cavity, Int. J. Heat Fluid Flow 14 (1993) 260–267.

[10] A. Mezrhab, L. Bchir, Radiation-natural convection interactions in partitioned cavities, Int. J. Num. Methods Heat Fluid Flow 8 (1998) 781–799.

[11] A. Mezrhab, L. Bchir, Radiation-natural convection interactions in partitioned cavities, Int. J. Num. Methods Heat Fluid Flow 9 (1999) 186–203.

[12] A. Mezrhab, H. Bouali, H. Amaoui, M. Bouzidi, Computation of combined natural convection and radiation heat transfer in a cavity having a square body at its center, Appl. Energy 83 (2006) 1004–1023.

[13] R. Siegel, J.R. Howell, Thermal Radiation Heat Transfer, second ed., Hemisphere Publishing Corporation, Washington, 1981.

[14] S.V. Patankar, Numerical Heat Transfer and Fluid Flow, Hemisphere Publishing Corporation, New York, 1980.

[15] G. de Vahl Davis, Natural convection of air in a square cavity: A benchmark solution, Int. J. Numer. Methods Fluids 3 (1983) 249–264.